

---

# PRUNEVID: VISUAL TOKEN PRUNING FOR EFFICIENT VIDEO LARGE LANGUAGE MODELS

Xiaohu Huang<sup>1</sup>      Hao Zhou<sup>2</sup>      Kai Han<sup>1†</sup>

<sup>1</sup> Visual AI Lab, The University of Hong Kong

<sup>2</sup> Department of Computer Vision Technology (VIS), Baidu Inc.

huangxiaohu@connect.hku.hk      zhouh156@mail.ustc.edu.cn      kaihanx@hku.hk

## ABSTRACT

In this paper, we introduce PruneVid, a visual token pruning method designed to enhance the efficiency of multi-modal video understanding. Large Language Models (LLMs) have shown promising performance in video tasks due to their extended capabilities in comprehending visual modalities. However, the substantial redundancy in video data presents significant computational challenges for LLMs. To address this issue, we introduce a training-free method that 1) minimizes video redundancy by merging spatial-temporal tokens, and 2) leverages LLMs’ reasoning capabilities to selectively prune visual features relevant to question tokens, enhancing model efficiency. We validate our method across multiple video benchmarks, which demonstrate that PruneVid can prune over 80% tokens while maintaining competitive performance combined with different model networks. This highlights its superior effectiveness and efficiency compared to existing pruning methods. Code: <https://github.com/Visual-AI/PruneVid>

## 1 INTRODUCTION

Large Language Models (LLMs) (Achiam et al., 2023; Yang et al., 2024; Touvron et al., 2023) have significantly advanced multi-modal understanding owing to their exceptional reasoning capabilities and proficiency in following instructions. Within the realm of video understanding, recent studies (Li et al., 2023c; Lin et al., 2023; Zhang et al., 2023; Li et al., 2024b; 2023a; Xu et al., 2024a; Wang et al., 2024a) have capitalized on the use of pre-trained LLMs as foundational models to address video question-answering tasks. However, the redundancy inherent in video content can lead to significant computational expenses for LLMs due to the quadratic complexity of attention mechanisms. Consequently, effectively reducing the number of video tokens while preserving model performance emerges as an intriguing area of research.

Previous approaches attempt to address this challenge in various ways. LLaMA-VID (Li et al., 2023c) proposes compressing each frame into two distinct tokens: context and content tokens. However, this method necessitates extensive pretraining and fine-tuning phases, which limits its broader applicability with readily available video LLMs. Alternatively, LLaVA-PruMerge (Shang et al., 2024) leverages the correlation between the [CLS] token and patch tokens within CLIP (Radford et al., 2021) to identify important visual tokens and merges other less important ones. Yet, this approach does not consider the relevance of the selected tokens to the questions being asked, potentially selecting tokens that are unrelated to the task at hand. In a related vein, methods like Look-M (Wan et al., 2024) and Elastic Cache (Liu et al., 2024d) employ Key-Value (KV) cache eviction strategies (Zhang et al., 2024; Liu et al., 2024c) to merge the KV cache for multi-modal inputs. These strategies prioritize retaining text tokens or treating visual and textual tokens equally without explicitly identifying the informative visual tokens. Moreover, eviction-based methods require encoding all visual tokens during the prefilling stage, which becomes inefficient when handling long visual sequences. Recently, FastV (Chen et al., 2025) has leveraged attention patterns in LLMs to prune visual tokens. However, it is not specifically tailored for video understanding and does not adequately address the reduction of video inputs.

---

<sup>†</sup>Corresponding author.

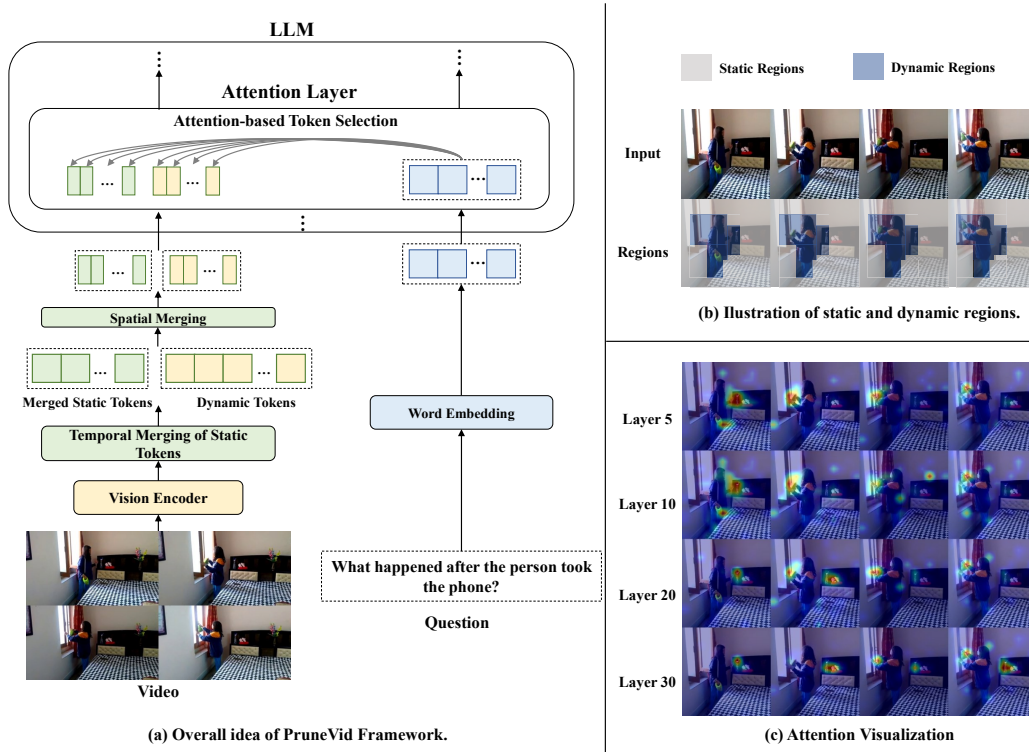


Figure 1: (a) PruneVid first identifies the static regions in the video that exhibit minimal variation, thereby compressing the redundancy of static tokens along the temporal dimension. It then further reduces spatial redundancy through compression in the spatial dimension. Subsequently, within the LLM, PruneVid utilizes question-to-visual attention scores to guide the selection of relevant visual tokens. (b) Static regions refer to areas with minimal change, while dynamic regions exhibit motion. Therefore, static regions can be compressed together along the temporal dimension. (c) Visualization of how attention evolves from shallow to deep layers (32 layers in total). The question tokens attend to semantically related visual regions (e.g., the hands and window) throughout different layers.

Building on the analysis presented above, we identify three essential criteria that an optimal pruning method for multi-modal video understanding ought to meet: (1) It should ideally be training-free, facilitating smooth integration with readily available models while reducing the need for extensive retraining or fine-tuning. (2) Inherent video redundancy needs to be reduced to save computations on tokens with similar representations along both spatial and temporal dimensions. (3) It is crucial to retain visual tokens specifically relevant to the given questions. This ensures the model maintains high performance while efficient and mitigates the risk of hallucinations when LLMs lack pertinent information (Huang et al., 2024).

To achieve our objectives, we present PruneVid, a training-free approach for pruning video tokens to achieve efficient video understanding. As shown in Fig. 1 (a), our method initially identifies static regions with minimal variation due to motion or camera movements, which could be interpreted as background (illustrated in Fig. 1 (b)). We merge these static tokens along the temporal dimension to reduce the computational burden from redundant temporal data. Next, we employ a clustering technique (Du et al., 2016) to merge similar spatial tokens for both static and dynamic regions. In the subsequent step within the LLM, we use attention scores between the question and video tokens in an intermediate layer to discern and preserve the discriminative visual tokens essential for answering the question, while pruning irrelevant ones. As depicted in Fig. 1 (c), attention visualizations consistently highlight crucial features, such as hand movements and related objects (e.g., a window), which are directly relevant to the question. This indicates that important visual regions can be effectively pinpointed using attention layers, benefiting from the LLM’s reasoning and instruction-following prowess. Additionally, for the KV caches from previous layers, we retain

---

the essential visual tokens and eliminate others, thus reducing computational demands during the decoding phase.

We integrate PruneVid with three video LLMs: PLLaVA (Xu et al., 2024a), ST-LLM (Liu et al., 2024b), and LLaVA-OneVision (Li et al., 2024a), and evaluate their performance on several video benchmarks, including MVBench (Li et al., 2024b), Video-MME (Fu et al., 2024), Egoschema (Mangalam et al., 2023), and VideoChatGPT-Bench (Maaz et al., 2023). Our extensive experiments demonstrate that PruneVid can prune over 80% of visual tokens with only minimal performance degradation in certain cases. Notably, our method can occasionally enhance model performance. Furthermore, it achieves competitive results compared to the baseline model while boosting inference speed—up to 1.55 times faster—reducing FLOPs by 74% to 80%, and minimizing GPU memory usage.

The main contributions of this paper are as follows: (1) We introduce PruneVid, a framework that efficiently prunes video tokens for video understanding without the need for retraining or fine-tuning, which can be seamlessly integrated with off-the-shelf video LLMs. (2) We introduce a token pruning method that minimizes video redundancy by merging static tokens over time and clustering spatially similar ones. Furthermore, our approach leverages attention scores between the question and video tokens within the LLM to retain only the visual tokens pertinent to answering the questions. (3) Extensive experiments are conducted across multiple benchmarks to demonstrate that PruneVid can consistently achieve superior efficiency and effectiveness with different video LLMs compared to existing approaches.

## 2 RELATED WORK

### 2.1 VIDEO LARGE LANGUAGE MODEL

Recent advancements in Video LLMs focus on enabling LLMs to comprehend video content. These approaches are broadly categorized into training-free methods and training-required methods.

For training-free approaches (Wu, 2024; Kim et al., 2024; Xu et al., 2024b), they directly adapt the image LLMs for video tasks. FreeVA (Wu, 2024) compacts frame features for LLM processing, and IG-VLM (Kim et al., 2024) merges frames into a single grid, simplifying video-to-image conversion. SF-LLaVA (Xu et al., 2024b) uses a SlowFast (Feichtenhofer et al., 2019) network design, balancing detailed spatial analysis with broad temporal scope efficiently within existing LLM token limits. These methods are ingeniously simple but are limited to handling only brief video clips due to their reliance on the inherent abilities of LLMs to understand temporal sequences.

Conversely, training-required Video LLMs improve comprehension by using extensive video datasets. Models like Video-ChatGPT (Maaz et al., 2023), Video-LLaVA (Lin et al., 2023), and PLLaVA (Xu et al., 2024a) extend Image LLMs with video-specific tuning, greatly enhancing complex video understanding. Other approaches, such as VideoChat2 (Li et al., 2024b), VILA (Lin et al., 2024), Tarsier Wang et al. (2024a), Chat-UniVi (Jin et al., 2024), LLaMA-VID (Li et al., 2023c), and ST-LLM Liu et al. (2024b), optimize token usage, refine training protocols, advance vision-audio integration, or use dynamic masking, thereby advancing video content analysis. Recently, LLaVA-OneVision (Li et al., 2024a) expanded the LLaVA (Liu et al., 2024a) architecture to incorporate more visual signals, achieving strong performance on video benchmarks.

Unlike the methods mentioned above, PruneVid aims to enhance the efficiency of existing video LLMs without additional training, which can be applied to both training-free and training-required methods.

### 2.2 VISUAL TOKEN PRUNING

Due to the quadratic computational complexity inherent in attention mechanisms, optimizing efficiency through token pruning becomes essential. This optimization highlights a crucial distinction between methods designed for vision-centric and multi-modal tasks.

DynamicViT (Rao et al., 2021) employs a prediction module to selectively prune less important tokens, thereby streamlining the model’s efficiency in processing visual data. Similarly, FastViT (Vasu et al., 2023) reduces architectural complexity and memory demands through a novel token mixing

operation, catering specifically to vision-only models. Further contributing to this domain, Token Merging (ToMe) (Bolya et al., 2023) merges tokens via token matching, while SPViT (Kong et al., 2022) introduces a method for softly aggregating redundant tokens into a single ‘package token’, efficiently preserving essential information while minimizing computational load.

Shifting away from vision-centric methods, LLaVA-Prumerge focuses on pruning visual tokens in multi-modal tasks. By employing an adaptive token reduction strategy, which utilizes CLIP’s inherent attention characteristics (Radford et al., 2021), LLaVA-Prumerge improves multi-modal understanding efficiency. FastV (Chen et al., 2025) addresses the inefficiency of visual attention patterns by pruning visual tokens with lower attention weights relative to the [EOS] token.

However, previous methods lack a specific focus on multi-modal video understanding. In contrast, this paper presents PruneVid, designed to eliminate redundancy in videos while utilizing LLMs to identify relevant video tokens for question answering. This approach enhances model efficiency without compromising performance.

### 3 METHOD

Our method is designed to efficiently process video data by minimizing redundancy in visual tokens before inputting them into the LLM and identifying question-relevant visual tokens within the LLM. In this section, we introduce the necessary preliminaries and provide a detailed explanation of our method.

#### 3.1 PRELIMINARIES

##### 3.1.1 PRE-FILLING STAGE

In the pre-filling stage, the model processes the input question tokens and visual tokens to construct the initial representations and prepare the key-value (KV) caches for attention computations. Let  $\mathbf{X}_q \in \mathbb{R}^{N_q \times C}$  denote the question tokens, where  $N_q$  is the length of the question and  $C$  is the channel dimension.

After the token merging, we obtain a compressed set of visual tokens  $\tilde{\mathbf{X}}_v \in \mathbb{R}^{N'_v \times C}$ , where  $N'_v$  is the reduced number of visual tokens. The combined input sequence  $\mathbf{X} \in \mathbb{R}^{(N_q+N'_v) \times C}$  is formed by concatenating the question tokens and the merged visual tokens. The model employs a Transformer architecture with  $L$  layers. In each layer  $l$ , the self-attention mechanism computes queries  $\mathbf{Q}^{(l)}$ , keys  $\mathbf{K}^{(l)}$ , and values  $\mathbf{V}^{(l)}$  through linear projections of the input.

Based on this, the attention scores are computed using scaled dot-product attention with causal masking to prevent attending to future positions:

$$\mathbf{A}^{(l)} = \text{Softmax} \left( \frac{\mathbf{Q}^{(l)}(\mathbf{K}^{(l)})^\top}{\sqrt{C}} + \mathbf{m} \right), \quad (1)$$

where  $\mathbf{m} \in \mathbb{R}^{(N_q+N'_v) \times (N_q+N'_v)}$  is a causal mask with entries  $m_{ij} = -\infty$  if position  $i < j$  (future positions) and 0 otherwise.

The KV caches  $\mathbf{KV}^{(l)} = (\mathbf{K}^{(l)}, \mathbf{V}^{(l)})$  are stored for each layer  $l$  to facilitate efficient computation during decoding.

##### 3.1.2 DECODING STAGE

In the decoding stage, the model generates the answer tokens autoregressively, utilizing the stored KV caches from the pre-filling stage. At each decoding step, given the previously generated tokens, the model computes the necessary representations to predict the next token. By using the KV caches, the model efficiently attends to the input sequence without recomputing the attention for the entire sequence. This process reduces computational overhead and speeds up the generation of the response.

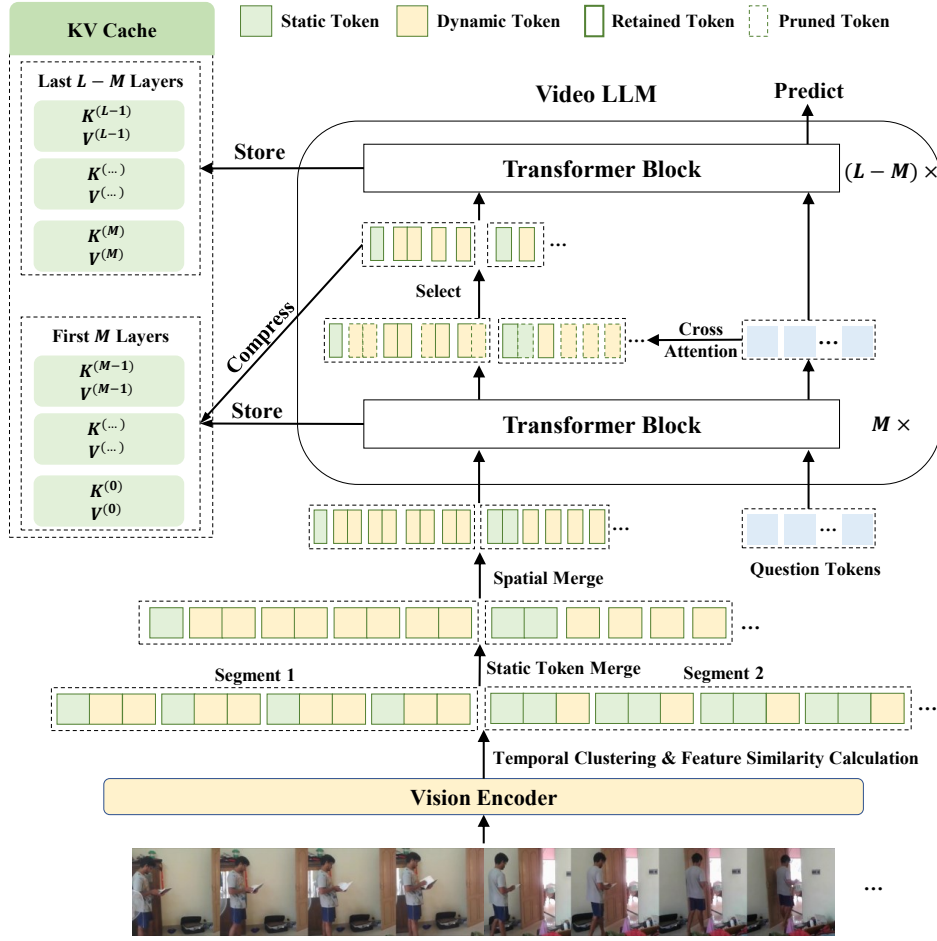


Figure 2: Illustration of the PruneVid framework. We begin by segmenting the video into different scenes and then decouple the video tokens into static and dynamic ones. Next, we compress the static tokens along the temporal dimension and merge similar tokens in the spatial dimension to further reduce redundancy. Afterward, by using the question-to-video attention weights learned from an intermediate layer, we determine which tokens should be pruned to improve efficiency.

### 3.2 SPATIAL-TEMPORAL TOKEN MERGING

As depicted in Fig. 2, given an input video consisting of  $T$  frames, we first extract visual tokens from each frame using a visual encoder. Let  $\mathbf{X}_v^{(t)} \in \mathbb{R}^{N_v \times C}$  denote the visual tokens for frame  $t$ , where  $N_v$  is the number of tokens per frame. The complete set of visual tokens for the video is then  $\mathbf{X}_v = \{\mathbf{X}_v^{(1)}, \mathbf{X}_v^{(2)}, \dots, \mathbf{X}_v^{(T)}\}$ .

To identify temporal segments with different scenes in the video, we perform temporal clustering based on the visual content. We compute the average pooled feature  $\mathbf{f}^{(t)} \in \mathbb{R}^C$  for each frame  $t$  by averaging over its tokens. Using the features  $\{\mathbf{f}^{(1)}, \dots, \mathbf{f}^{(T)}\}$ , we employ the Density Peaks Clustering with  $k$ -Nearest Neighbors (DPC-KNN) (Du et al., 2016) algorithm to group the frames into  $B$  temporal segments  $\{\mathcal{T}_1, \mathcal{T}_2, \dots, \mathcal{T}_B\}$ . Here,  $B$  is linearly related to  $T$  with the coefficient  $\gamma$ , and each segment  $\mathcal{T}_b$  comprises a subset of consecutive frames with similar content.

Within each temporal segment  $\mathcal{T}_b$ , we analyze the spatial tokens across the frames to identify static tokens—tokens that remain largely unchanged throughout the segment. For each spatial location  $i$  (where  $1 \leq i \leq N_v$ ), we extract the sequence of tokens  $\{\mathbf{X}_v^{(t)}(i) \mid t \in \mathcal{T}_b\}$  and compute the feature similarities between every pair of tokens in this sequence. Specifically, for tokens at times  $t$  and  $t'$

within  $\mathcal{T}_b$ , the similarity is measured using cosine similarity  $s_i^{(t,t')}$ :

$$s_i^{(t,t')} = \frac{\mathbf{X}_v^{(t)}(i)^\top \mathbf{X}_v^{(t')}(i)}{\|\mathbf{X}_v^{(t)}(i)\| \|\mathbf{X}_v^{(t')}(i)\|}. \quad (2)$$

We then compute the average similarity for each spatial location  $i$  within the segment:

$$\bar{s}_i = \frac{2}{|\mathcal{T}_b|(|\mathcal{T}_b| - 1)} \sum_{t,t' \in \mathcal{T}_b, t < t'} s_i^{(t,t')}. \quad (3)$$

Tokens with average similarity above a threshold  $\tau$  are considered static:

$$\mathcal{I}_{\text{static}} = \{i \mid \bar{s}_i \geq \tau\}. \quad (4)$$

For these static tokens, we perform temporal averaging within the segment to compress temporal redundancy:

$$\tilde{\mathbf{X}}_v^{(b)}(i) = \frac{1}{|\mathcal{T}_b|} \sum_{t \in \mathcal{T}_b} \mathbf{X}_v^{(t)}(i), \quad \forall i \in \mathcal{I}_{\text{static}}. \quad (5)$$

The dynamic tokens, corresponding to  $\mathcal{I}_{\text{dynamic}} = \{1, \dots, N_v\} \setminus \mathcal{I}_{\text{static}}$ , are retained without temporal averaging.

To further reduce spatial redundancy, we perform spatial clustering within each frame also using the DPC-KNN algorithm. We apply this clustering separately to the static and dynamic tokens. For frame  $t$ , we cluster the tokens  $\{\mathbf{X}_v^{(t)}(i) \mid i \in \mathcal{I}_{\text{static}}\}$  and  $\{\mathbf{X}_v^{(t)}(i) \mid i \in \mathcal{I}_{\text{dynamic}}\}$  to obtain clusters  $\mathcal{C}_1^{(t)}, \dots, \mathcal{C}_{C_s}^{(t)}$  for the static tokens and  $\mathcal{D}_1^{(t)}, \dots, \mathcal{D}_{C_d}^{(t)}$  for the dynamic tokens. For both static and dynamic tokens, the cluster number is linearly related to  $|\mathcal{I}_{\text{static}}|$  and  $|\mathcal{I}_{\text{dynamic}}|$  with the coefficient  $\beta$ . We average the tokens within each cluster to represent them with a single token  $\tilde{\mathbf{X}}_v^{(t)}(c)$  for  $c = 1, \dots, C_s$  in the static clusters, and similarly for the dynamic clusters  $\tilde{\mathbf{X}}_v^{(t)}(d)$  for  $d = 1, \dots, C_d$ .

After these merging operations, we obtain a reduced set of visual tokens  $\tilde{\mathbf{X}}_v$  with significantly less redundancy. The merged visual tokens for the entire video are then collected and concatenated to form the final token sequence to be input to the LLM:

$$\tilde{\mathbf{X}}_v = \bigcup_{b=1}^B \left( \tilde{\mathbf{X}}_v^{(b)} \right), \quad (6)$$

where  $\tilde{\mathbf{X}}_v^{(b)}$  contains the merged tokens from segment  $\mathcal{T}_b$ .

### 3.3 LLM-GUIDED TOKEN SELECTION

We further reduce the visual tokens by leveraging the LLM’s internal attentions to select the most relevant tokens with respect to the given question.

Consider the LLM with  $L$  layers. During the pre-filling stage, we target the  $M$ -th layer, where  $1 \leq M \leq L$ , to compute cross-attention weights between the question tokens and the merged visual tokens to obtain a measure of relevance.

At the  $M$ -th layer, we calculate the attention scores  $\mathbf{A}^{(M)} \in \mathbb{R}^{(N_q+N'_v) \times (N_q+N'_v)}$  according to Eq. (1). To obtain the cross-attention scores between question and visual tokens, we extract a sub-matrix  $\mathbf{A}_{qv}^{(M)} \in \mathbb{R}^{N_q \times N'_v}$  as follows:

$$\mathbf{A}_{qv}^{(M)} = \mathbf{A}^{(M)}[N'_v :, : N'_v], \quad (7)$$

where  $\mathbf{A}^{(M)}[N'_v :, : N'_v]$  selects the attention scores from the question tokens to the visual tokens.

Next, we compute the maximum attention values  $\mathbf{a}_v \in \mathbb{R}^{N'_v}$  for each visual token by applying max pooling over all question tokens. This approach captures the most informative tokens, as not all question tokens are equally important:

$$\mathbf{a}_v = \max_{i=1}^{N_q} \mathbf{A}_{qv}^{(M)}(i, :).$$

We then sort the attention scores in descending order and select the top  $\alpha\%$  of visual tokens. The set of indices for the selected tokens is represented by  $\mathcal{S}$  and is defined as:

$$\mathcal{S} = \{j \in \{1, \dots, N'_v\} \mid \text{Rank}(\mathbf{a}_v(j)) \leq \lceil \alpha N'_v \rceil\}, \quad (8)$$

where  $\text{Rank}(\mathbf{a}_v(j))$  indicates the rank of  $\mathbf{a}_v(j)$  within the sorted attention scores, and  $\lceil \cdot \rceil$  denotes the ceiling function.

By focusing on the top  $\alpha\%$  tokens, we align the model’s attention with the most question-relevant visual information. To finalize the pre-filling stage, we combine the selected visual tokens with the question tokens, enabling processing in the remaining  $(L - M)$  layers of the LLM. The KV vectors derived from the retained visual tokens and question tokens, calculated in the last  $(L - M)$  layers, are stored in the KV cache for the decoding process.

### 3.3.1 COMPRESSED KEY-VALUE CACHES

To reduce memory and computational costs during the decoding stage, we compress the KV caches stored from the previous  $M$  layers by retaining only the selected visual tokens. For each layer  $l$  ( $1 \leq l \leq M$ ), the original key and value matrices for the visual tokens are  $\mathbf{K}_v^{(l)} \in \mathbb{R}^{N'_v \times C}$  and  $\mathbf{V}_v^{(l)} \in \mathbb{R}^{N'_v \times C}$ .

We create the compressed key and value matrices  $\tilde{\mathbf{K}}_v^{(l)}$  and  $\tilde{\mathbf{V}}_v^{(l)}$  by selecting the rows corresponding to the indices in  $\mathcal{S}$ :

$$\tilde{\mathbf{K}}_v^{(l)} = \mathbf{K}_v^{(l)}[\mathcal{S},:], \quad \tilde{\mathbf{V}}_v^{(l)} = \mathbf{V}_v^{(l)}[\mathcal{S},:], \quad (9)$$

where  $\mathbf{K}_v^{(l)}[\mathcal{S},:]$  and  $\mathbf{V}_v^{(l)}[\mathcal{S},:]$  denote the selection of rows corresponding to the indices in  $\mathcal{S}$ .

Similarly, we adjust the key and value matrices for the entire sequence by combining the question tokens and the selected visual tokens:

$$\tilde{\mathbf{K}}^{(l)} = \left[ \tilde{\mathbf{K}}_v^{(l)}; \mathbf{K}_q^{(l)} \right], \quad \tilde{\mathbf{V}}^{(l)} = \left[ \tilde{\mathbf{V}}_v^{(l)}; \mathbf{V}_q^{(l)} \right], \quad (10)$$

where  $\mathbf{K}_q^{(l)}$  and  $\mathbf{V}_q^{(l)}$  are the key and value matrices for the question tokens. By compressing the KV caches, we effectively reduce the sequence length from  $N_q + N'_v$  to  $N_q + |\mathcal{S}|$ , where  $|\mathcal{S}|$  represents the total number of selected visual tokens.

This compression significantly reduces the memory requirements and computational complexity during decoding, enabling efficient processing of long video sequences within the LLM framework.

## 4 EXPERIMENT

### 4.1 DATASETS AND EVALUATION METRICS

**Generic Multi-Choice VideoQA.** MVbench (Li et al., 2024b) encompasses 20 temporally challenging tasks that cannot be addressed using a single frame. Each task includes 200 test samples, formatted as multiple-choice VideoQA. These samples require the model to choose the correct answer from several provided options.

**Long-form Multi-Choice VideoQA.** We conduct evaluations of our models using two well-regarded benchmarks for long-form video benchmarks: Video-MME (Fu et al., 2024) and Egoschema (Mangalam et al., 2023). In these evaluations, the models are tasked with selecting the correct answer from multiple-choice options.

**Text Generation.** VideoChatGPT-Bench, introduced by (Maaz et al., 2023), focuses on five aspects: Correctness of Information (CI), Detail Orientation (DO), Contextual Understanding (CU), Temporal Understanding (TU), and Consistency (CO). For evaluation, we use GPT-3.5-Turbo-0125 for scoring.

Table 1: Performance and efficiency comparison across different methods and benchmarks. The best results of pruning methods are **bolded**.

Method	Retained Ratio	FLOPs ( $\times$ )	MVBench	VideoMME	EgoSchema	VideoChatGPT-Bench					
						Subset / Fullset	TU	CU	CO	DO	CI
PLLaVA	100.0%	1.00 $\times$	46.6	44.4	47.8 / 42.6	2.33	3.62	2.93	2.86	3.21	2.99
PLLaVA w/ FastV	30.0%	0.33 $\times$	46.1	43.6	46.2 / 41.0	2.38	3.49	2.89	2.76	3.14	2.93
PLLaVA w/ Prumerge	55.7%	0.53 $\times$	45.6	43.8	45.2 / 40.4	2.34	3.52	2.90	2.76	3.15	2.93
PLLaVA w/ Look-M	20.0%	1.00 $\times$	46.6	44.3	47.0 / 42.3	2.28	3.41	2.75	2.65	3.00	2.82
PLLaVA w/ Ours	<b>16.2%</b>	<b>0.23<math>\times</math></b>	<b>47.6</b>	<b>45.0</b>	<b>49.0 / 42.6</b>	<b>2.44</b>	<b>3.51</b>	<b>2.99</b>	<b>2.78</b>	<b>3.20</b>	<b>2.98</b>
ST-LLM	100.0%	1.00 $\times$	54.9	42.0	56.2 / 45.6	2.46	3.46	2.66	2.63	3.08	2.86
ST-LLM w/ FastV	30.0%	0.37 $\times$	42.9	34.5	48.0 / 38.5	2.01	2.23	1.55	1.94	1.69	1.88
ST-LLM w/ Look-M	20.0%	1.00 $\times$	54.0	40.6	54.0 / 44.5	2.35	3.41	2.60	2.51	3.01	2.78
ST-LLM w/ Ours	<b>15.1%</b>	<b>0.26<math>\times</math></b>	<b>54.3</b>	<b>41.4</b>	<b>54.6 / 44.7</b>	<b>2.40</b>	<b>3.43</b>	<b>2.63</b>	<b>2.60</b>	<b>3.04</b>	<b>2.82</b>
LLaVA-OneVision	100.0%	1.00 $\times$	58.0	58.2	62.0 / 60.0	2.75	3.70	3.39	2.97	3.50	3.26
LLaVA-OneVision w/ FastV	30.0%	0.30 $\times$	57.2	57.6	62.6 / 60.0	2.65	3.61	3.28	2.85	3.39	3.16
LLaVA-OneVision w/ Prumerge	55.2%	0.49 $\times$	52.9	56.7	62.2 / 60.0	2.72	3.64	<b>3.32</b>	<b>2.94</b>	3.44	3.21
LLaVA-OneVision w/ Look-M	20.0%	1.00 $\times$	57.0	58.0	62.0 / <b>59.8</b>	2.71	3.70	3.29	2.89	3.44	3.21
LLaVA-OneVision w/ Ours	<b>17.0%</b>	<b>0.20<math>\times</math></b>	<b>57.5</b>	<b>58.6</b>	<b>62.6 / 59.5</b>	<b>2.73</b>	<b>3.72</b>	3.28	<b>2.94</b>	<b>3.51</b>	<b>3.24</b>

## 4.2 BASELINES

To evaluate the effectiveness of our approach, we compare it with three visual token pruning methods: LLaVA-PruMerge (Shang et al., 2024), Look-M (Wan et al., 2024), and FastV (Chen et al., 2025). LLaVA-PruMerge utilizes attention score sparsification within CLIP to identify crucial tokens and employs an outlier detection method to adaptively determine the optimal pruning ratio. Conversely, Look-M extends the concept of text-only KV cache compression to a multi-modal context by implementing strategies for evicting text-prior KV pairs and merging them through a pivotal merging strategy. Additionally, FastV (Chen et al., 2025) uses attention weights to prune visual tokens with low attention scores. To ensure a fair comparison, we use the official implementations of these methods and apply them to video benchmarks.

## 4.3 IMPLEMENTATION DETAILS

All experiments are conducted on NVIDIA A100 GPUs with 80GB of memory. We implement PruneVid, LLaVA-PruMerge, Look-M, and FastV on three video LLMs: PLLaVA (Xu et al., 2024a), ST-LLM (Wang et al., 2024a), and LLaVA-OneVision (Li et al., 2024a). LLaVA-PruMerge is incompatible with ST-LLM, so it is excluded from related comparisons. As per the official settings, the input frames are set to 16 for both PLLaVA and ST-LLM, and 32 for LLaVA-OneVision. For the VideoChatGPT-Bench, ST-LLM uses 64 input frames. Besides, The threshold  $\tau$  is set to 0.8, the temporal segment ratio  $\gamma$  is 0.25, and the cluster ratio  $\beta$  is 0.5. Across all benchmarks, the token selection ratio  $\alpha$  is 0.4, and attention calculations use the 10th layer ( $M$ ). For FastV, we prune the tokens at the 2nd layer and set the retained ratio to 0.3 to achieve roughly comparable FLOPs to our method. Additionally, the FLOPs in the experiments are measured in relation to the visual tokens in the LLM.

## 4.4 MAIN RESULT

As illustrated Tab. 1, our method consistently achieves the best performance in almost all cases compared to existing pruning methods (FastV, Prumerge, and Look-M) while retaining fewer tokens and achieving lower FLOPs. For instance, on PLLaVA, our approach retains only 16.2% of tokens yet surpasses the performance of other pruning methods and even the baseline model under MVBench, VideoMME, and Egoschema. A similar pattern is observed for ST-LLM and LLaVA-OneVision, where our method maintains robust performance with retained ratios as low as 15.1% and 17.0%, respectively, across all benchmarks. This underscores the versatility of our approach in balancing accuracy with a substantial reduction in computational overhead.

Moreover, while Prumerge also maintains competitive accuracy on some models, it fails to do so with substantially reduced token budgets. Similarly, although Look-M can achieve decent performance, it requires using the vanilla attention implementation for all layers, resulting in relatively low



Table 2: Efficiency comparison for visual token pruning methods. TTFT stands for time-to-first-token, which is commonly used for evaluating the efficiency of LLMs.

Method	FLOPs ( $\times$ )	TTFT Speed Up ( $\times$ )	GPU Mem	Accuracy
Baseline	1.00 $\times$	1.00 $\times$	20G	46.6
Baseline w/FastV	0.33 $\times$	1.15 $\times$	19G	46.1
Baseline w/Prumerge	0.53 $\times$	1.32 $\times$	19G	45.6
Baseline w/Look-M	1.00 $\times$	0.15 $\times$	35G	46.6
Baseline w/Ours	<b>0.23</b> $\times$	<b>1.55</b> $\times$	<b>17G</b>	<b>47.6</b>

efficiency. Additionally, we find that FastV struggles to maintain consistent performance across different models. For instance, while it performs well on PLLaVA and LLaVA-OneVision, its accuracy on ST-LLM is unsatisfactory, indicating a lack of robustness across diverse architectures. In contrast, our method effectively adapts by identifying and preserving only the most informative tokens for video understanding, thereby delivering strong overall performance with significantly reduced computational costs.

#### 4.5 DIAGNOSTIC STUDY

In this section, we conduct a diagnostic study based on the PLLaVA model for efficiency comparison, hyper-parameter investigations, and qualitative visualizations.

**Efficiency Analysis.** As shown on Tab. 2, We compare multiple visual token pruning methods with respect to FLOPs, TTFT speed-up, GPU memory usage, and accuracy. Overall, FastV and Prumerge both demonstrate notable FLOPs reduction and moderate speed gains, though their influence on accuracy remains slightly adverse. By contrast, Look-M manages to preserve accuracy comparable to the baseline but incurs a very low TTFT speed up and escalates GPU memory to a high level, suggesting that its underlying layer-wise strategy increases overhead. In contrast, our proposed method achieves the most efficient balance by yielding the fastest TTFT speed up, the largest FLOPs reduction, the smallest memory footprint, and the highest accuracy, clearly underscoring the advantages of our token pruning approach over existing techniques.

**Ablation Study on Token Selection Ratio  $\alpha$  and the Position of Pruning Layer  $M$ .** As shown in Fig. 3 (a), we observe that when pruning attention from the 10th layer onward, model accuracy, despite minor fluctuations, gradually saturates. Therefore, selecting  $M$  as 10 for token pruning results in lower computational costs compared to pruning at later layers. Additionally, we find that using a larger  $\alpha$  does not necessarily yield better results. For instance, when  $M$  is 10, an  $\alpha$  of 0.4 achieves better accuracy than 0.5, as retaining more tokens may introduce irrelevant information, adversely affecting the outcome.

**Ablation Study on threshold  $\tau$  and temporal segment ratio  $\gamma$ .** As depicted in Fig. 3 (b), we observe that performance consistently improves as  $\tau$  increases from 0.6 to 0.8, while the performance between  $\tau = 0.8$  and  $\tau = 0.9$  remains similar. Given that setting  $\tau = 0.8$  allows the model to merge more tokens along the temporal dimension, resulting in a higher compression ratio, we select  $\tau = 0.8$ . Concerning the temporal segment ratio  $\gamma$ , the variation in its values does not significantly affect performance. We found that both  $\gamma = 0.25$  and  $\gamma = 1.0$  deliver good results across the two datasets. However, since  $\gamma = 1.0$  treats each input frame as an individual segment, which hinders effective temporal merging of static tokens, we choose to set  $\gamma$  to 0.25.

**Ablation Study on threshold  $\tau$  and spatial merging ratio  $\beta$ .** As shown in Fig. 3 (c), the performance is comparable for  $\tau$  values of 0.8 and 0.9, with  $\tau = 0.8$  being slightly superior, which is a similar phenomenon as in Fig. 3 (b). Regarding the parameter  $\beta$ , setting it to 0.5 provides the optimal accuracy. This is because a smaller  $\beta$  leads to overly aggressive merging of spatial tokens, which degrades performance. On the other hand, setting  $\beta$  to 1.0 is unable to merge redundant tokens, which also adversely affects performance.

**Side-by-side Visualizations of Attention Maps and Token Selection.** In Fig. 4, we present a side-by-side comparison demonstrating how our model selects tokens guided by attention scores, highlighting the LLM’s strength in focusing on informative regions related to the questions.

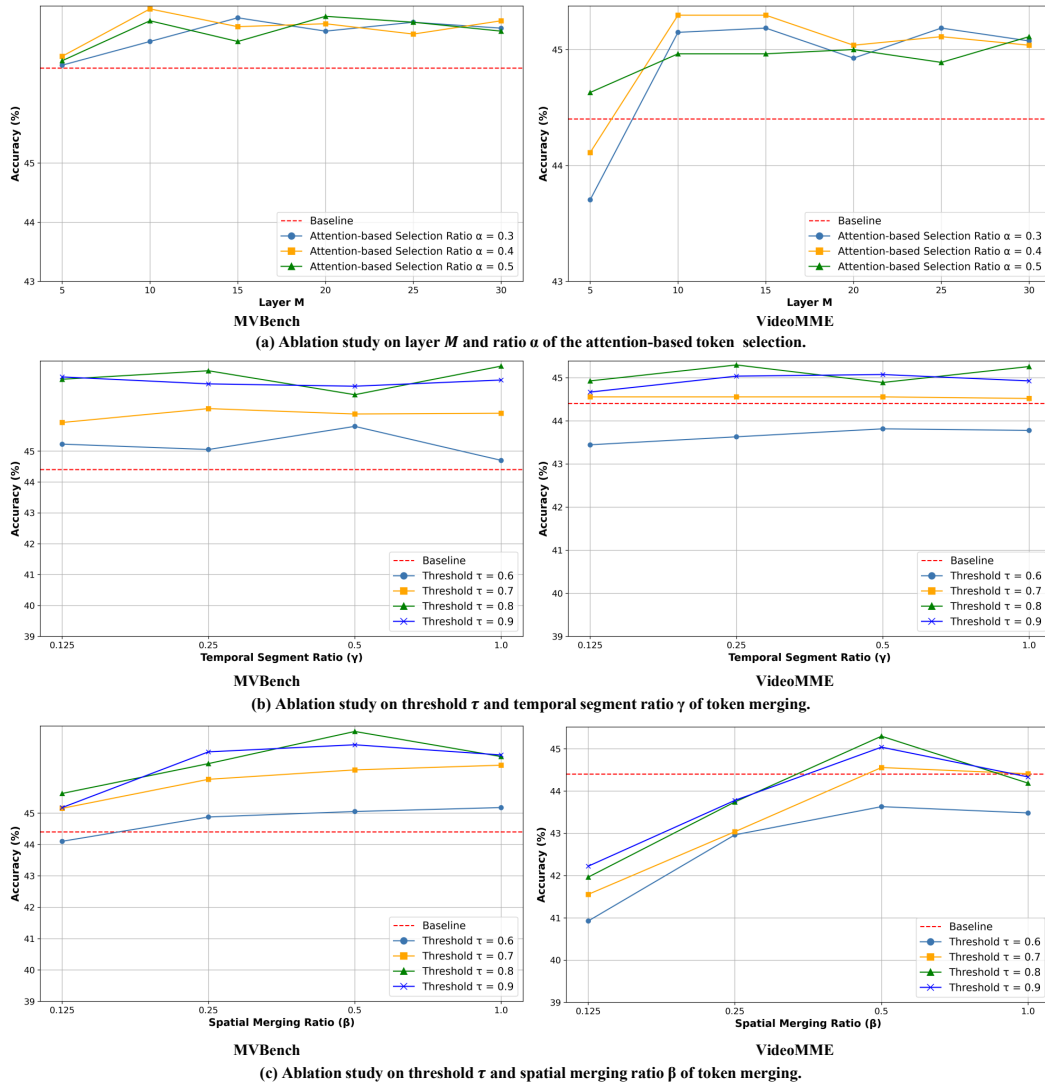


Figure 3: The ablation study of hyper-parameters.

Below, we provide detailed analyses on how our model leverages the *reasoning capabilities of LLMs* to locate relevant visual regions that are not explicitly mentioned in the questions:

Fig. 4 (a): The model identifies the key object mentioned in the question, the *blanket*, and uses the temporal cue (*after*) from the question to locate additional relevant visual elements, such as objects on the table and the person’s hand movements in frames 2, 6, and 7. These details are not directly provided in the question and are inferred through the model’s reasoning abilities.

Fig. 4 (b): The model accurately detects the action of the person holding food in frames 7 and 8, and infers that the presence of a *bag* the person puts down is relevant for answering the question, even though the *bag* is not mentioned. This demonstrates the model’s ability to reason about relevant objects based on contextual cues.

Fig. 4 (c): Despite the absence of any mention of a *book* in the question, the model correctly identifies critical visual regions related to the *book* by reasoning over the visual content and context provided.



Figure 4: Visualization of the question-to-visual attentions and token selection of PruneVid.

---

Fig. 4 (d): The model focuses on the person’s hand movements, which are crucial for answering the question. Even though the question does not emphasize hand motions, the model infers the importance of these actions through reasoning.

These examples showcase how our model utilizes LLM reasoning to identify and focus on pertinent visual information that is not explicitly described in the questions.

## 5 CONCLUSION

We present PruneVid, a training-free visual token pruning method that enhances efficiency in multi-modal video understanding. By reducing video redundancy through merging static tokens over time and clustering similar spatial tokens, PruneVid minimizes the number of tokens processed. It leverages attention mechanisms within LLMs to retain only the visual tokens relevant to questions, ensuring high performance while reducing computational overhead. Experiments across multiple benchmarks demonstrate that PruneVid can prune over 80% of visual tokens while maintaining, or even improving, model performance. By eliminating the need for retraining or fine-tuning, PruneVid offers a practical and efficient solution that integrates seamlessly with existing video LLMs.

## ACKNOWLEDGMENTS

This work is supported by Hong Kong Research Grant Council - Early Career Scheme (Grant No. 27208022), National Natural Science Foundation of China (Grant No. 62306251), and HKU Seed Fund for Basic Research.

## REFERENCES

- Josh Achiam, Steven Adler, Sandhini Agarwal, Lama Ahmad, Ilge Akkaya, Florencia Leoni Aleman, Diogo Almeida, Janko Altschmidt, Sam Altman, Shyamal Anadkat, et al. Gpt-4 technical report. *Arxiv e-prints*, 2023.
- Daniel Bolya, Cheng-Yang Fu, Xiaoliang Dai, Peizhao Zhang, Christoph Feichtenhofer, and Judy Hoffman. Token merging: Your vit but faster. *ICLR*, 2023.
- Liang Chen, Haozhe Zhao, Tianyu Liu, Shuai Bai, Junyang Lin, Chang Zhou, and Baobao Chang. An image is worth 1/2 tokens after layer 2: Plug-and-play inference acceleration for large vision-language models. In *eccv*, 2025.
- Mingjing Du, Shifei Ding, and Hongjie Jia. Study on density peaks clustering based on k-nearest neighbors and principal component analysis. *Knowledge-Based Systems*, 2016.
- Christoph Feichtenhofer, Haoqi Fan, Jitendra Malik, and Kaiming He. Slowfast networks for video recognition. In *ICCV*, 2019.
- Chaoyou Fu, Yuhan Dai, Yongdong Luo, Lei Li, Shuhuai Ren, Renrui Zhang, Zihan Wang, Chenyu Zhou, Yunhang Shen, Mengdan Zhang, et al. Video-mme: The first-ever comprehensive evaluation benchmark of multi-modal llms in video analysis. *Arxiv e-prints*, 2024.
- Wen Huang, Hongbin Liu, Minxin Guo, and Neil Zhenqiang Gong. Visual hallucinations of multi-modal large language models. *Arxiv e-prints*, 2024.
- Peng Jin, Ryuichi Takanobu, Wancai Zhang, Xiaochun Cao, and Li Yuan. Chat-univi: Unified visual representation empowers large language models with image and video understanding. In *CVPR*, 2024.
- Wonkyun Kim, Changin Choi, Wonseok Lee, and Wonjong Rhee. An image grid can be worth a video: Zero-shot video question answering using a vlm. *Arxiv e-prints*, 2024.
- Zhenglun Kong, Peiyan Dong, Xiaolong Ma, Xin Meng, Wei Niu, Mengshu Sun, Xuan Shen, Geng Yuan, Bin Ren, Hao Tang, et al. Spvit: Enabling faster vision transformers via latency-aware soft token pruning. In *ECCV*, 2022.

- 
- Bo Li, Yuanhan Zhang, Dong Guo, Renrui Zhang, Feng Li, Hao Zhang, Kaichen Zhang, Peiyuan Zhang, Yanwei Li, Ziwei Liu, et al. Llava-onevision: Easy visual task transfer. *arXiv preprint arXiv:2408.03326*, 2024a.
- KunChang Li, Yinan He, Yi Wang, Yizhuo Li, Wenhai Wang, Ping Luo, Yali Wang, Limin Wang, and Yu Qiao. Videochat: Chat-centric video understanding. *Arxiv e-prints*, 2023a.
- Kunchang Li, Yali Wang, Yizhuo Li, Yi Wang, Yinan He, Limin Wang, and Yu Qiao. Unmasked teacher: Towards training-efficient video foundation models. 2023b.
- Kunchang Li, Yali Wang, Yinan He, Yizhuo Li, Yi Wang, Yi Liu, Zun Wang, Jilan Xu, Guo Chen, Ping Luo, et al. Mvbench: A comprehensive multi-modal video understanding benchmark. In *CVPR*, 2024b.
- Yanwei Li, Chengyao Wang, and Jiaya Jia. Llama-vid: An image is worth 2 tokens in large language models. In *CVPR*, 2023c.
- Bin Lin, Bin Zhu, Yang Ye, Munan Ning, Peng Jin, and Li Yuan. Video-llava: Learning united visual representation by alignment before projection. *Arxiv e-prints*, 2023.
- Ji Lin, Hongxu Yin, Wei Ping, Pavlo Molchanov, Mohammad Shoeybi, and Song Han. Vila: On pre-training for visual language models. In *CVPR*, 2024.
- Haotian Liu, Chunyuan Li, Qingyang Wu, and Yong Jae Lee. Visual instruction tuning. *nips*, 2024a.
- Ruyang Liu, Chen Li, Haoran Tang, Yixiao Ge, Ying Shan, and Ge Li. St-llm: Large language models are effective temporal learners. *Arxiv e-prints*, 2024b.
- Zichang Liu, Aditya Desai, Fangshuo Liao, Weitao Wang, Victor Xie, Zhaozhuo Xu, Anastasios Kyrillidis, and Anshumali Shrivastava. Scissorhands: Exploiting the persistence of importance hypothesis for llm kv cache compression at test time. *NeurIPS*, 2024c.
- Zuyan Liu, Benlin Liu, Jiahui Wang, Yuhao Dong, Guangyi Chen, Yongming Rao, Ranjay Krishna, and Jiwen Lu. Efficient inference of vision instruction-following models with elastic cache. *Arxiv e-prints*, 2024d.
- Muhammad Maaz, Hanoona Rasheed, Salman Khan, and Fahad Shahbaz Khan. Video-chatgpt: Towards detailed video understanding via large vision and language models. *Arxiv e-prints*, 2023.
- Kartikeya Mangalam, Raiymbek Akshulakov, and Jitendra Malik. Egoschema: A diagnostic benchmark for very long-form video language understanding. *NeurIPS*, 2023.
- Alec Radford, Jong Wook Kim, Chris Hallacy, Aditya Ramesh, Gabriel Goh, Sandhini Agarwal, Girish Sastry, Amanda Askell, Pamela Mishkin, Jack Clark, et al. Learning transferable visual models from natural language supervision. In *ICML*, 2021.
- Yongming Rao, Wenliang Zhao, Benlin Liu, Jiwen Lu, Jie Zhou, and Cho-Jui Hsieh. Dynamicvit: Efficient vision transformers with dynamic token sparsification. *NeurIPS*, 2021.
- Yuzhang Shang, Mu Cai, Bingxin Xu, Yong Jae Lee, and Yan Yan. Llava-prumerge: Adaptive token reduction for efficient large multimodal models. *Arxiv e-prints*, 2024.
- Hugo Touvron, Thibaut Lavril, Gautier Izacard, Xavier Martinet, Marie-Anne Lachaux, Timothée Lacroix, Baptiste Rozière, Naman Goyal, Eric Hambro, Faisal Azhar, et al. Llama: Open and efficient foundation language models. *Arxiv e-prints*, 2023.
- Pavan Kumar Anasosalu Vasu, James Gabriel, Jeff Zhu, Oncel Tuzel, and Anurag Ranjan. Fastvit: A fast hybrid vision transformer using structural reparameterization. In *ICCV*, 2023.
- Zhongwei Wan, Ziang Wu, Che Liu, Jinfang Huang, Zhihong Zhu, Peng Jin, Longyue Wang, and Li Yuan. Look-m: Look-once optimization in kv cache for efficient multimodal long-context inference. *Arxiv e-prints*, 2024.
- Jiawei Wang, Liping Yuan, and Yuchen Zhang. Tarsier: Recipes for training and evaluating large video description models. *Arxiv e-prints*, 2024a.

- 
- Mengmeng Wang, Jiazheng Xing, and Yong Liu. Actionclip: A new paradigm for video action recognition. *Arxiv e-prints*, 2021.
- Yi Wang, Kunchang Li, Xinhao Li, Jiashuo Yu, Yanan He, Guo Chen, Baoqi Pei, Rongkun Zheng, Jilan Xu, Zun Wang, et al. Internvideo2: Scaling video foundation models for multimodal video understanding. *Arxiv e-prints*, 2024b.
- Wenhao Wu. Freeva: Offline mllm as training-free video assistant. *Arxiv e-prints*, 2024.
- Lin Xu, Yilin Zhao, Daquan Zhou, Zhijie Lin, See Kiong Ng, and Jiashi Feng. Pllava: Parameter-free llava extension from images to videos for video dense captioning. *Arxiv e-prints*, 2024a.
- Mingze Xu, Mingfei Gao, Zhe Gan, Hong-You Chen, Zhengfeng Lai, Haiming Gang, Kai Kang, and Afshin Dehghan. Slowfast-llava: A strong training-free baseline for video large language models. *Arxiv e-prints*, 2024b.
- An Yang, Baosong Yang, Binyuan Hui, Bo Zheng, Bowen Yu, Chang Zhou, Chengpeng Li, Chengyuan Li, Dayiheng Liu, Fei Huang, et al. Qwen2 technical report. *Arxiv e-prints*, 2024.
- Hang Zhang, Xin Li, and Lidong Bing. Video-llama: An instruction-tuned audio-visual language model for video understanding. *Arxiv e-prints*, 2023.
- Zhenyu Zhang, Ying Sheng, Tianyi Zhou, Tianlong Chen, Lianmin Zheng, Ruisi Cai, Zhao Song, Yuandong Tian, Christopher Ré, Clark Barrett, et al. H2o: Heavy-hitter oracle for efficient generative inference of large language models. *NeurIPS*, 2024.

## A APPENDIX

**Attention Map Comparison.** In Fig. 5 and Fig. 6, we include comparisons between our LLM’s attention maps and those of several strong video encoders, including UMT (Li et al., 2023b), ActionCLIP (Wang et al., 2021), and InternVideo2 (Wang et al., 2024b). The results show that, unlike these models, the question-to-vision attentions in the LLM accurately focus on visual tokens that are pertinent to the question. In contrast, the other models often struggle to pinpoint key tokens and may focus on irrelevant objects or background elements. These observations suggest that LLMs possess a unique ability to align visual information with linguistic context through their reasoning capabilities, which is not simply a byproduct of standard attention mechanisms in typical video encoders.

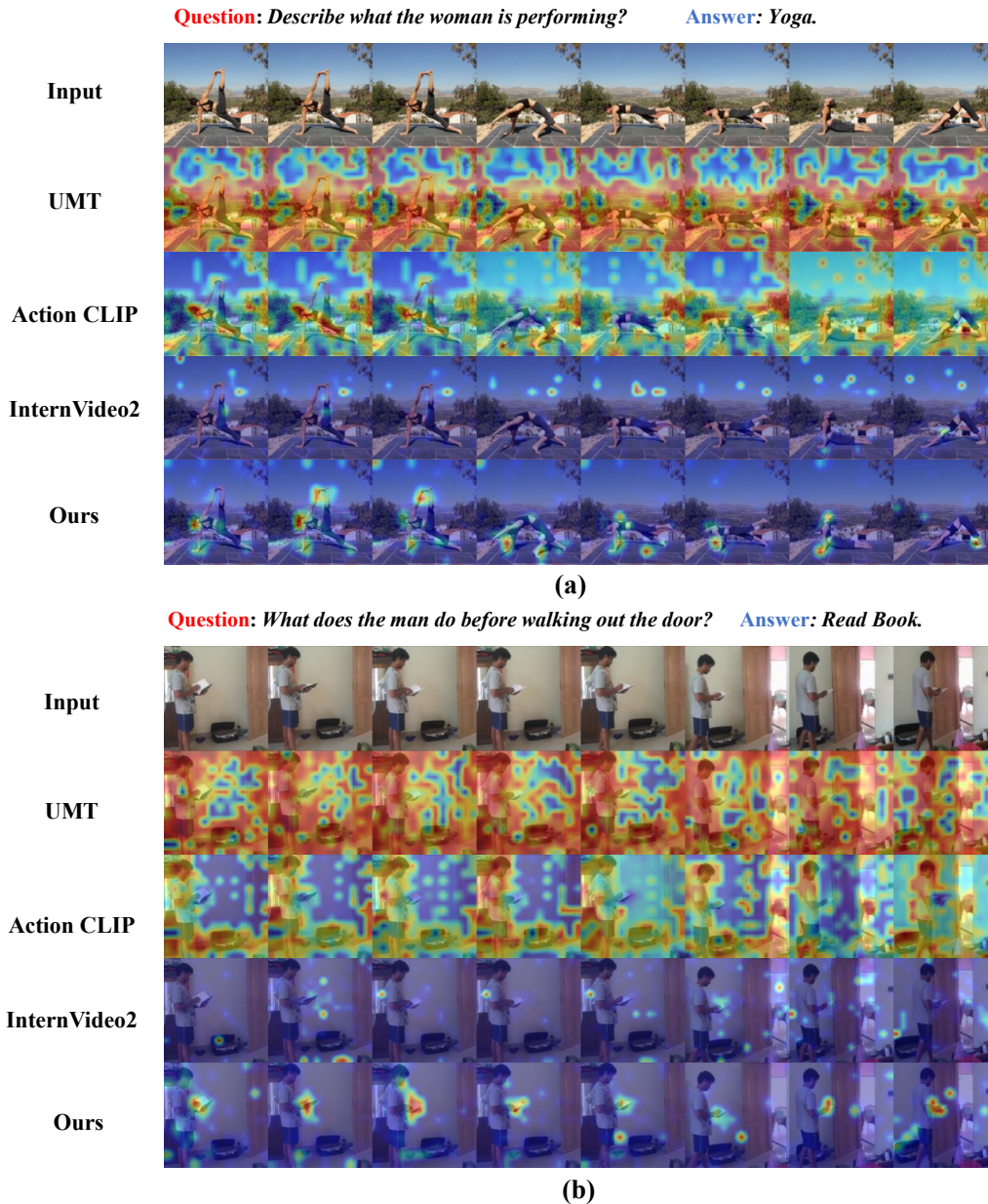


Figure 5: Attention map comparison of video encoders and our method.



(c)

**Question:** *What happened before the person held the food?*      **Answer:** *Put down the bag.*



(d)

Figure 6: Attention map comparison of video encoders and our method.